

Influence of Hydrostatic Pressure on Dynamics and Spatial Distribution of Protein Partial Molar Volume: Time-Resolved Surficial Kirkwood-Buff Approach

Isseki Yu,^{*,†,‡} Tomohiro Tasaki,[†] Kyoko Nakada,[†] and Masataka Nagaoka^{‡,§}

Department of Chemistry and Biological Science, College of Science and Engineering, Aoyama Gakuin University, 5-10-1 Fuchinobe, Sagamihara, Kanagawa 229-8558, Japan, Graduate School of Information Science, Nagoya University, Furo-cho, Chikusa-ku, Nagoya 464-8601, Japan, and CREST, Japan Science and Technology Agency, Japan

Received: May 12, 2010; Revised Manuscript Received: August 14, 2010

The influence of hydrostatic pressure on the partial molar volume (PMV) of the protein apomyoglobin (AMb) was investigated by all-atom molecular dynamics (MD) simulations. Using the time-resolved Kirkwood–Buff (KB) approach, the dynamic behavior of the PMV was identified. The simulated time average value of the PMV and its reduction by 3000 bar pressurization correlated with experimental data. In addition, with the aid of the surficial KB integral method, we obtained the spatial distributions of the components of PMV to elucidate the detailed mechanism of the PMV reduction. New R -dependent PMV profiles identified the regions that increase or decrease the PMV under the high pressure condition. The results indicate that besides the hydration in the vicinity of the protein surface, the outer space of the first hydration layer also significantly influences the total PMV change. These results provide a direct and detailed picture of pressure induced PMV reduction.

1. Introduction

The influence of hydrostatic pressure on protein function should be examined from the viewpoint of partial molar volume (PMV), which represents the contribution that a protein makes to the overall volume of the solution. PMV and the compressibility of proteins under many chemical or physical conditions have been analyzed by thermodynamic measurements.^{1–7} In addition to experimental efforts, statistical-mechanical methods have also been applied to provide mainly the time average value of the PMV for a target protein (or the target protein conformation).⁸

We have developed a methodology to extract the time dependency of the PMV from the trajectory of all atom molecular dynamics (MD) simulations.⁹ On the basis of the Kirkwood–Buff (KB) theory,^{10,11} instantaneous atomic positions of water molecules are utilized to calculate the instantaneous PMV. This approach provides the time dependency of the PMV, which reflects not only the protein structural fluctuation but also the *dynamics of hydration*.

In this work, using apomyoglobin (AMb) as the target protein, we monitored the dynamic behavior of the PMV in response to pressurization. We chose 3000 bar, which represents a typical value used in high pressure conditions.¹² Time average, standard deviation, and the isothermal compressibility of the PMV were compared with experimental values. Furthermore, using our own surficial KB integral method,^{9,13,14} the spatial distribution of the components of the PMV were analyzed to determine the influence of hydration on the PMV change. Detailed analysis of the pressure induced PMV reduction was examined by comparing the R -dependent PMV profiles of AMb between atmospheric and high pressure conditions.

This article is organized as follows: Initially, the computational methods and the model systems are explained. Precise numerical results are provided and discussed in the Results and Discussion. Finally, the present study is summarized in the Concluding Remarks.

2. Computational Methods

2.1. Surficial Kirkwood–Buff Integral. The Kirkwood–Buff (KB) integral^{10,11} of solvent component s around a certain solute molecule α is defined as follows,

$$G_{\alpha s} = \int [g_s(\mathbf{r}) - 1] d\mathbf{r} \quad (1)$$

where $g_s(\mathbf{r})$ is the number density of the s at position \mathbf{r} , normalized by the density in the bulk phase. The integral should be taken in whole three-dimensional space around α . $G_{\alpha s}$ connects the microscopic solvent distribution $g_s(\mathbf{r})$ to the PMV (see eq 5).

To understand the spatial distribution of $G_{\alpha s}$ based on numerous MD derived protein snapshots, the integral form of eq 1 is inconvenient to use because the solute flexibly changes its conformation. To overcome this problem, we have introduced another type of R -dependent KB integral, $G_{\alpha s}^S(R)$, the surficial KB integral^{9,13,14} as follows,

$$G_{\alpha s}^S(R) = \langle G_{\alpha s}^S(R, t) \rangle_T = \left\langle \int_{r=0}^{r=R} \left\{ \frac{1}{\rho_s(\infty)} \left(\frac{\partial N_{\alpha s}(r, t)}{\partial r} / \frac{\partial U_\alpha(r, t)}{\partial r} \right) - 1 \right\} S_\alpha(r, t) dr \right\rangle_T \quad (2)$$

where $\langle \dots \rangle_T$ denotes the time-average, defined as $1/T \int_0^T (\dots) dt$. $U_\alpha(r, t)$ and $S_\alpha(r, t)$ are the volume and the surface area of the hypothetical spatial region $v_\alpha(r, t)$ around the solute molecule α . The boundary of $v_\alpha(r, t)$ is defined as the surface whose distance to the nearest atom site of the solute molecule α is r . Schematic representation of $v_\alpha(r, t)$, $U_\alpha(r, t)$, and $S_\alpha(r, t)$ is shown

* Corresponding author. E-mail: yu@chem.aoyama.ac.jp. Tel: +81-42-759-6296. Fax: +81-42-759-6493.

† Aoyama Gakuin University.

‡ Japan Science and Technology Agency.

§ Nagoya University.

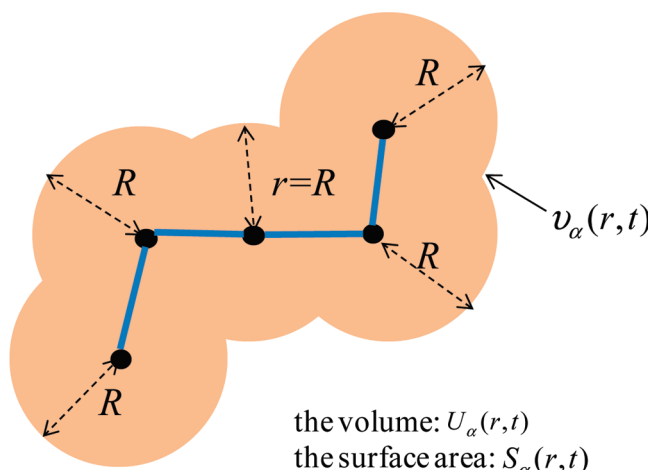


Figure 1. Schematic representation of the integration range in the surficial KB integral $G_{\alpha s}^S(R)$ for the solute molecule α (blue lines). The boundary of the integration range $v_{\alpha}(r,t)$ is defined as the surface whose minimum distance to any atom center (black circles) of the solute is r and is represented as the circumference of the orange region. The volume and the surface area of $v_{\alpha}(r,t)$ are denoted by $U_{\alpha}(r,t)$ and $S_{\alpha}(r,t)$, respectively.

In Figure 1. Here, the distance r from (or between) certain atom(s) is that from (or between) the center of the atom(s). $N_{\alpha s}(r,t)$ is the instantaneous coordination number of atoms in the solvent component s within the region $v_{\alpha}(r,t)$.⁹ $\rho_s(\infty)$ is the atomic number density of s in the bulk phase (for example, if s represents water, $\rho_s(\infty)$ is 3 times larger than the density of water molecules in the bulk since each water molecule is composed of three atoms). Currently, the atomic number density of s at r (normalized by the density in the bulk phase), $\bar{\rho}_{\alpha s}(r)$, is defined as

$$\bar{\rho}_{\alpha s}(r) = \left\langle \frac{1}{\rho_s(\infty)} \left(\frac{\partial N_{\alpha s}(r,t)}{\partial r} / \frac{\partial U_{\alpha}(r,t)}{\partial r} \right) \right\rangle_T \quad (3)$$

Both $G_{\alpha s}^S(R)$ and conventional $G_{\alpha s}$ show exactly the same constant value when their integration range reaches the bulk solvent phase as follows,

$$\lim_{R \rightarrow \infty} G_{\alpha s}^S(R) = G_{\alpha s} \quad (4)$$

$G_{\alpha s}^S(R)$ enables a clearer understanding of the profile of solvent distribution and the related thermodynamic quantities as functions of the distance from the solute surface.

2.2. Time Dependency and R Dependency of the Partial Molar Volume. PMV of the solute molecule α in the solvent component s , $V_{\alpha s}$, is expressed by using $G_{\alpha s}$ as follows,^{8,9,11}

$$V_{\alpha s} = k_B T \chi_T^0 - G_{\alpha s} \quad (5)$$

where χ_T^0 is the isothermal compressibility of the pure solvent. The first term, $k_B T \chi_T^0$, corresponds to the ideal volume contribution and comes from the translational degree of freedom of the solute molecule α . The value of the ideal term is only about $1.0 \text{ cm}^3 \text{ mol}^{-1}$ and therefore can usually be ignored when large solutes are considered.^{8,9}

Using the surficial KB integral, $G_{\alpha s}^S(R)$, the R -dependent PMV of the solute molecule α , $V_{\alpha s}(R)$, can be expressed as follows,

$$V_{\alpha s}(R) = \langle V_{\alpha s}(R,t) \rangle_T = \langle -G_{\alpha s}^S(R,t) \rangle_T \quad (6)$$

Taking R to an infinite distance, the instantaneous PMV of the solute molecule α , $V_{\alpha s}(t)$, and their time average value, $V_{\alpha s}$, is expressed as follows,

$$V_{\alpha s} = \langle V_{\alpha s}(t) \rangle_T = \langle \lim_{R \rightarrow \infty} V_{\alpha s}(R,t) \rangle_T \quad (7)$$

The increment of $V_{\alpha s}(R)$ at distance r , $\delta V_{\alpha s}(r)$, is defined as follows,

$$\delta V_{\alpha s}(r) = V_{\alpha s}(r + \Delta r/2) - V_{\alpha s}(r - \Delta r/2) \quad (8)$$

The standard deviation of PMV, $\sigma_{\alpha s}^V$, is calculated as follows,

$$\sigma_{\alpha s}^V = \sqrt{\langle (V_{\alpha s}(t) - \langle V_{\alpha s}(t) \rangle_T)^2 \rangle_T} \quad (9)$$

2.3. Molecular Dynamics Simulations. MD calculations were performed using the AMBER10 program.¹⁵ The force field parameter set, ff03,¹⁶ was used for all the molecules in the present systems. The crystal structure of sperm whale myoglobin was retrieved from the PDB, entry 104M. The initial coordinate for the AMb was taken from the crystal structure with the removal of the heme group. MD simulation of the 3000 bar pressurization to AMb was performed as follows. Initially, AMb was set in a periodic boundary box filled with 24 649 TIP4P water molecules.¹⁷ After the system was initially equilibrated, a 5 ns production MD run was executed at 1 bar and 298 K. This MD simulation was named MD_L. Using the final atomic positions and velocity distributions at 3, 4, and 5 ns in MD_L as starting conditions of the system, three different 5 ns MD runs were performed at 3000 bar and 298 K. These three MD simulations under the high pressure conditions were named MD_{H1}, MD_{H2}, and MD_{H3}. All the MD simulations were performed under the NPT conditions, using the Berendsen algorithm¹⁸ for temperature and pressure regulation. Trajectories were numerically integrated by the velocity Verlet method with a time step of 2.0 fs. The electrostatic interactions were treated by the particle-mesh Ewald (PME) method.¹⁹ Bonds involving hydrogen atoms were constrained by the SHAKE method.²⁰

3. Results and Discussion

3.1. Structural Changes to Apomyoglobin by Pressurization. To understand the influence of pressurization on the protein structure, changes in the radius of gyration (R_g) and the solvent accessible surface area (SASA) of AMb were analyzed. As a result, R_g under 3000 bar decreased by ~1.1%, implying that pressurization slightly compacts the protein structure. Similar reductions in R_g have also been observed in both theoretical and experimental works.^{21,22} Conversely, no noticeable influence of pressurization on the SASA was observed.

3.2. Partial Molar Volume Reduction. The time histories of the instantaneous PMV of AMb under atmospheric (1 bar) and high pressure (3000 bar) conditions are presented in Figure 2a. The averaged time history for PMVs in MD_{H1}, MD_{H2}, and MD_{H3} is also shown in Figure 2b. Conformations of AMb in MD_L and MD_{H1-3} are collectively denoted as "L" (Low) and "H" (High), respectively. The solvent in this study, i.e., water, is denoted as "w". All the atoms in water molecules are equally utilized for calculations. Instantaneous PMVs of AMb in both conditions, $V_{Lw}(t)$ and $V_{Hw}(t)$, defined at infinite distance from

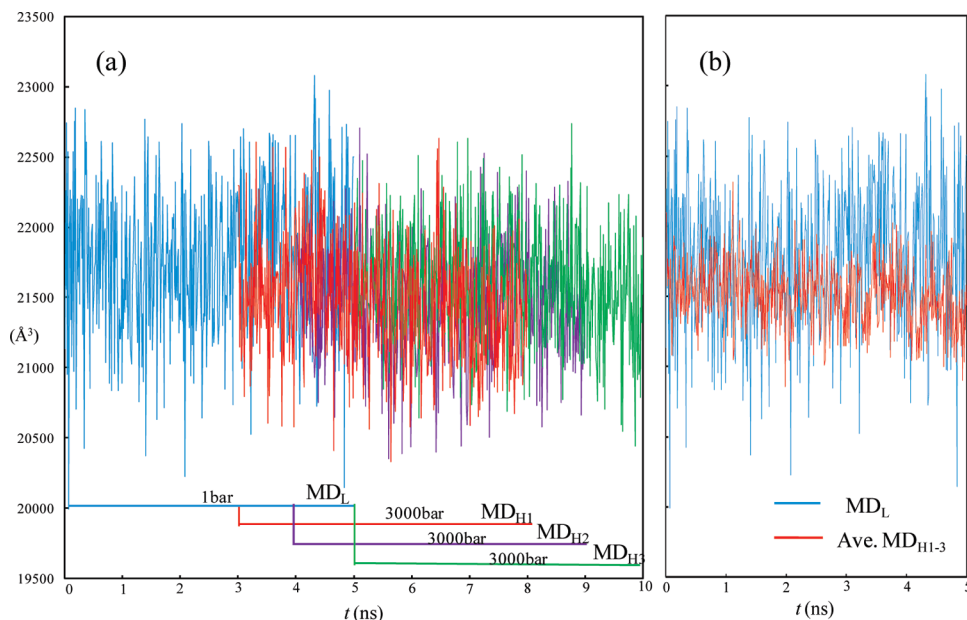


Figure 2. (a) Time histories of PMV under atmospheric (1 bar) condition (MD_L, blue) and under the high pressure (3000 bar) condition (MD_{H1}, red; MD_{H2}, violet; MD_{H3}, green). At the bottom of the figure, the time duration of each MD simulation is depicted as lines with the same color as the PMV trajectory. (b) Averaged time history for PMVs in MD_{H1}, MD_{H2} and MD_{H3} (red) superimposed on the time history of the PMV in the MD_L (blue).

TABLE 1: Time Average Values of the PMV (V_{Lw} , V_{Hw}), PMV Change (ΔV), the Isothermal Compressibility ($\bar{\beta}_T(P)$) of AMb, and the Standard Deviations of the PMV (σ_{Lw}^V , σ_{Hw}^V)^a

	V_{Lw} (Å³)	V_{Hw} (Å³)	ΔV (Å³)	$\bar{\beta}_T(P)$ (Mbar⁻¹)	σ_{Lw}^V (Å³)	σ_{Hw}^V (Å³)
calc	21778 (1 bar)	21479 (3000 bar)	-299 (1 → 3000 bar)	4.6 (1500 bar)	511 (1 bar)	396 (3000 bar)
exp	22016 ^b (1 bar)			13.1 ^b (1 bar)	106 ^b (1 bar)	
	21312 ^c (1 bar)		-125 ^d (1 → 1200 bar) -166 ^e (1 → 700 bar)	4.8 ^d (600) 5.4 ^e (700 bar) 11.0 ^e (1 bar) 17.5 ^f (1 bar)		

^a Related experimental values at room temperature are also shown in the “exp” line. ^b Experimental V_{Lw} , $\bar{\beta}_T(P)$, and σ_{Lw}^V for whale myoglobin, taken from ref 2. ^c Experimental V_{Lw} , for SNase calculated from the specific volume of SNase (0.763 cm³ g⁻¹)⁶ and its molecular weight 16812 Da. ^d Experimental ΔV for apomyoglobin at 1200 bar (taken from ref 12), and $\bar{\beta}_T(P)$ estimated by ΔV and eq 10. ^e Experimental ΔV and $\bar{\beta}_T(P)$ for SNase taken from ref 7. ΔV was estimated from the change in the specific volume of SNase by 700 bar pressurization (Figure 3 in ref 7). ^f Intrinsic compressibility of myoglobin subtracted from experimental $\bar{\beta}_T(P)$ data.²⁴

the solute (eq 7), are evaluated at $R = 12.0$ Å. For both conditions, snapshots with time intervals of 10 ps were extracted and utilized to analyze the time dependencies of PMVs. The isothermal compressibility of AMb at pressure P , $\bar{\beta}_T(P)$, was calculated as follows,

$$\bar{\beta}_T(P) = -\left\{ \frac{1}{(V_{\text{Lw}} + V_{\text{Hw}})/2} \right\} \{(V_{\text{Hw}} - V_{\text{Lw}})/(P_{\text{H}} - P_{\text{L}})\} \quad (10)$$

where P_{H} and P_{L} are the pressure of high and low pressure conditions, respectively, and P is the pressure at the center of P_{H} , and P_{L} ($P = P_{\text{L}} + (P_{\text{H}} - P_{\text{L}})/2$).

The time average and standard deviation of the PMV and isothermal compressibility of AMb under atmospheric (1 bar) conditions were calculated using 500 snapshots extracted from the entire time duration of the MD_L. In contrast, 3 × 300 (= 900) snapshots from the last 3 ns of three MD simulations, i.e., MD_{H1}, MD_{H2}, and MD_{H3}, were used to obtain those values under the high pressure (3000 bar) condition. The data are shown in the table with some experimental values.

V_{Lw} compared reasonably well with the experimental work for whale myoglobin,² implying that our MD simulation

appropriately reproduced the hydration of AMb under atmospheric condition. The theoretical V_{Lw} is also comparable to that of SNase,⁶ which has a sequence length similar to that for AMb. A remarkable reduction of the PMV was observed in response to 3000 bar pressurization. We obtained a PMV change $\Delta V = (V_{\text{Hw}} - V_{\text{Lw}}) = -299$ (Å³), which correlates with estimates using high-pressure NMR for AMb at 1200 bar $\Delta V = -125$ (Å³)¹² and densitometric measurements for SNase at 700 bar $\Delta V = -166$ (Å³).⁷

By using eq 10, we estimated the isothermal compressibility of AMb $\bar{\beta}_T(1500) = 4.6$ (Mbar⁻¹), which is close to that estimated by eq 10 and the experimental ΔV value obtained from high-pressure NMR for AMb $\bar{\beta}_T(600) = 4.8$ (Mbar⁻¹).¹² These are, however, linearly approximated values calculated by assigning two sets of (P , V_{aw}) data to eq 10. On the other hand, Winter and co-workers directly measured the pressure-volume profiles for SNase and obtained $\bar{\beta}_T(1) = 11.0$ (Mbar⁻¹) and $\bar{\beta}_T(700) = 5.4$ (Mbar⁻¹).⁷ The $\bar{\beta}_T(700)$ for SNase is slightly larger than the theoretical $\bar{\beta}_T(1500)$ for AMb. In addition, sound velocity measurements for myoglobin at 1 bar obtained $\bar{\beta}_T(1) = 13.1$ (Mbar⁻¹).² These lines of experimental and theoretical values indicate that $\bar{\beta}_T(P)$ s decrease at high pressure.

With the aid of an MD simulation, Dadarlat and Post developed a methodology to decompose the experimental $\bar{\beta}_T(P)$ into intrinsic

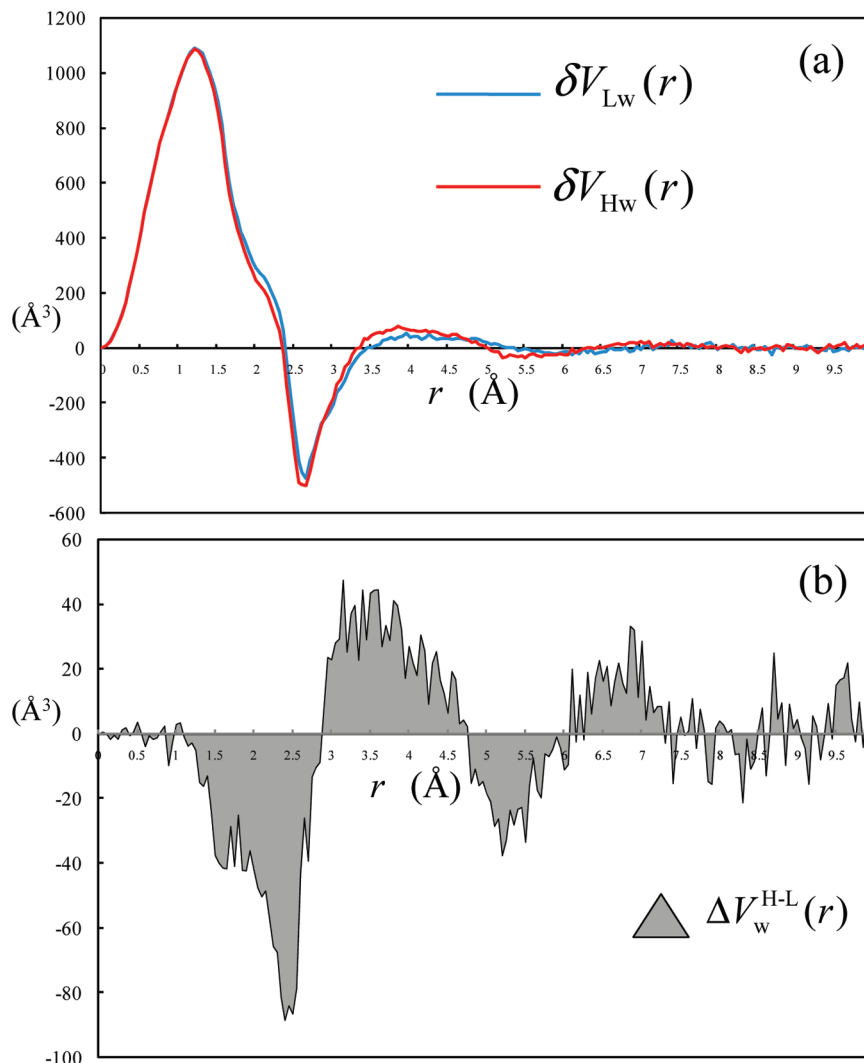


Figure 3. (a) Profiles of the PMV increment under atmospheric (1 bar) condition ($\delta V_{Lw}(r)$: blue) and under high pressure (3000 bar) condition ($\delta V_{Hw}(r)$: red) (in \AA^3). (b) Profile of the difference between $\delta V_{Hw}(r)$ and $\delta V_{Lw}(r)$. To obtain their numerical values, Δr (in eq 8) was set to 0.05\AA . A total of 1000 snapshots extracted from the last 1 ns of the MD_L (MD_{H3}) were utilized for the analysis of the atmospheric (high pressure) condition.

(van der Waals and void volume) and hydration shell contributions.^{23,24} They obtained the intrinsic compressibility of myoglobin as $17.5 (\text{Mbar}^{-1})$, which is remarkably larger than the experimental $\bar{\beta}_T(P)$, and showed that the hydration shell has negative contributions to the overall isothermal compressibility of myoglobin. Furthermore, from the fluctuation of the number of water molecules, they independently calculated the isothermal compressibility of the first hydration shell for trypsin as $47.2 (\text{Mbar}^{-1})$ and HEW lysozyme $41.6 (\text{Mbar}^{-1})$, which is 77 and 68% of the isothermal compressibility of the bulk water, respectively.²⁴ The rates are consistent with the sound velocity measurements.^{1,25} Because of the problem of the finite size effect in the convergence of the compressibility, it would be difficult to estimate $\bar{\beta}_T(P)$ for more microscopic regions using the fluctuation of the number of water molecules (the limits of convergence are discussed in ref 23). High-resolution quantitation for the position \mathbf{r} and pressure P dependence of the water compressibility $\bar{\beta}_T(\mathbf{r}, P)$ around the target protein is vitally needed.

As for the magnitude of the PMV fluctuation, we obtained $\sigma_{Lw}^V = 511 (\text{\AA}^3)$, which is remarkably larger than that estimated from the sound velocity measurement for whale myoglobin.² Because the integration range in the surficial KB integral accommodated a large enough distance to reach the bulk phase, the theoretical σ_{Lw}^V (derived with $R = 12 \text{\AA}$) should be influenced by the volume

fluctuation, i.e., compressibility of the TIP4P water molecules in the bulk phase. As discussed previously, the isothermal compressibility of the bulk (pure) water is considerably larger than that of the hydration water around the protein.^{1,24,25} Furthermore, the TIP4P water model is known to overestimate the isothermal compressibility of the bulk water.²⁶ In addition, the absence of the heme group in the MD simulations influences the structural fluctuations of AMb. These represent some of the factors that most likely give rise to the larger theoretical σ_{Lw}^V value over the experimental value for myoglobin.

3.3. Intrinsic Alteration in the Partial Molar Volume. To elucidate the detailed mechanism of the PMV reduction, the influence of pressurization on the spatial distribution of the components of the PMV around AMb were investigated. The R -dependent PMV increments (defined in eq 8) in both conditions, $\delta V_{Lw}(r)$ and $\delta V_{Hw}(r)$, are shown in Figure 3a. In addition, Figure 3b shows the difference between the two profiles defined as follows,

$$\Delta V_w^{H-L}(r) = \delta V_{Hw}(r) - \delta V_{Lw}(r) \quad (11)$$

The positive (negative) value in $\Delta V_w^{H-L}(r)$ indicates that the pressurization increases (decreases) the PMV at distance r from

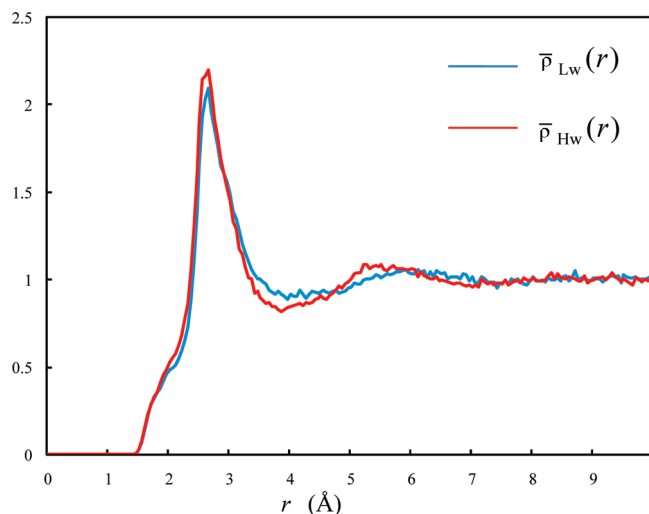


Figure 4. Profiles of the water atomic number density under the atmospheric (1 bar) condition $\bar{\rho}_{Lw}(r)$ (blue) and under the high pressure (3000 bar) conditions $\bar{\rho}_{Hw}(r)$ (red). Both $\bar{\rho}_{Lw}(r)$ and $\bar{\rho}_{Hw}(r)$ are normalized by the density in the bulk phase in each condition. A total of 1000 snapshots extracted from the last 1 ns of the MD_L (MD_{H3}) were used for the analysis of the atmospheric (high pressure) condition.

AMb. Figure 4 shows the profiles of water atomic number density, $\bar{\rho}_{aw}(r)$, defined in eq 3. Furthermore, the three-dimensional distributions of water atomic number density, $g_w(\mathbf{r})$, are also shown in Figure 5. Both $\bar{\rho}_{aw}(r)$ and $g_w(\mathbf{r})$ are normalized by the density in the bulk phase.

In Figure 3b, a sharp negative peak in $\Delta V_w^{H-L}(r)$ from $r \approx 1.0$ to 3.0 Å has an origin in the growth of the first peak in $\bar{\rho}_{Hw}(r)$ (Figure 4). Under the high pressure conditions, the first hydration layer should be denser, and some water molecules

penetrate into the interior of the protein to occupy the voids or cavities. Conversely, we have discovered an interesting PMV increment in $\Delta V_w^{H-L}(r)$ from $r \approx 3.0$ to 4.7 Å. This arises from the deepening of the first minimum of $\bar{\rho}_{Hw}(r)$ (Figure 4), implying that the water molecules are more strongly excluded from the region because of pressurization. In the three-dimensional distribution images (Figure 5), such regions (blue belts in Figure 5 (3)) spread like coral reefs to the outer spaces of the first hydration layer (green belts in Figure 5 (3)) and are more apparent with pressurization. From $r \approx 4.7$ Å, the fluctuation of $\Delta V_w^{H-L}(r)$ becomes smaller as r reaches the bulk phase. These intrinsic PMV alterations arise from the high pressure conditions employed: (i) the amplitude of the fluctuation in $\bar{\rho}_{Hw}(r)$ is larger than in $\bar{\rho}_{Lw}(r)$, and (ii) the positions of the first minimum and the second peak in $\bar{\rho}_{Hw}(r)$ shift slightly closer to the protein surface.

4. Concluding Remarks

We performed all-atom MD simulations of AMb responding to 3000 bar pressurization. With the aid of the time-resolved KB approach, the dynamic behavior of the PMV was identified directly from the MD trajectories. The time average value of the PMV and the isothermal compressibility compared reasonably well with those values obtained from experimental measurements; however, the fluctuation of the PMV was larger than the experimental data.

Furthermore, with the aid of the surficial KB integral method, we obtained the spatial distributions of the components of the PMV to elucidate the detailed mechanism of the PMV reduction in AMb. The profiles of the new R -dependent PMV, $\delta V_{Lw}(r)$ and $\delta V_{Hw}(r)$, identified the regions that increase or decrease the PMV under high pressure. The results indicate that besides changes in hydration in the vicinity of the protein surface, the

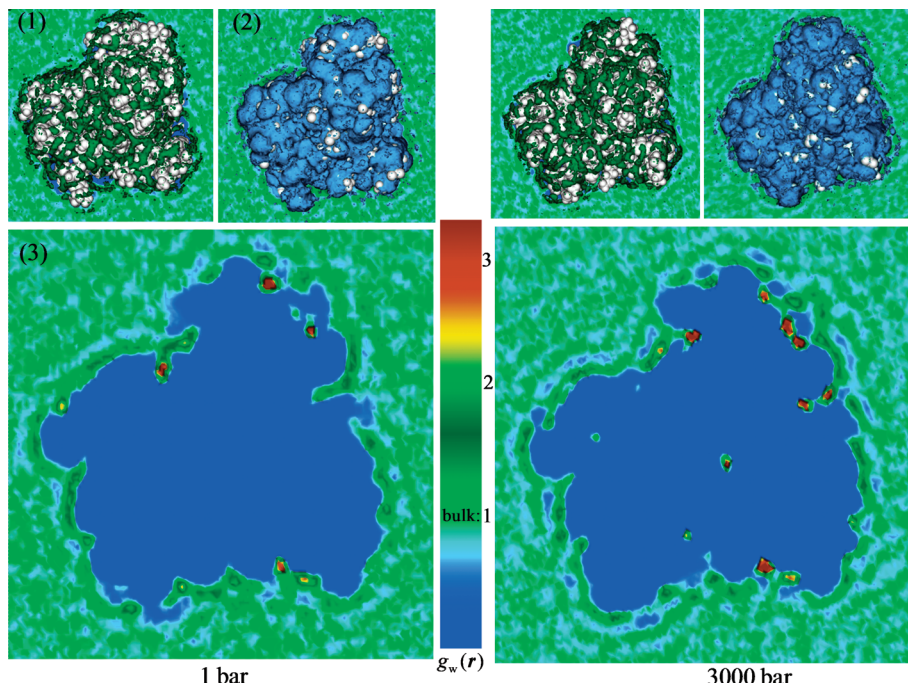


Figure 5. Three-dimensional distributions of the water atomic number density $g_w(\mathbf{r})$ under atmospheric conditions (left) and under high-pressure conditions (right). The color tone is normalized by the density in the bulk phase in each condition. Clockwise: (1) hydration sites reducing the PMV (green), in which $g_w(\mathbf{r})$'s are more than 1.4, are superimposed on the van der Waals expression of the AMb (white); (2) water exclusion sites increasing the PMV (blue), in which $g_w(\mathbf{r})$'s are less than 0.7; (3) the cross sectional view of $g_w(\mathbf{r})$. A total of 10 000 snapshots extracted from the last 1 ns of the MD_L (MD_{H3}) were used for the analysis of the atmospheric (high pressure) conditions. To obtain clear hydration structure images without constraining the protein conformation, all atomic positions at each snapshot (including water molecules) were translated and rotated to minimize the root-mean-square displacement (rmsd) of the protein conformations.

outer space of the first hydration layer also significantly influences the total PMV change. These results provide a direct and detailed picture of the pressure induced PMV reduction.

For AMb to reach the equilibrium structure under 3000 bar a significantly longer time scale of simulations would be required. Therefore, within the time duration explored in these simulations, we mainly focused on the influence of hydration changes on the PMV reduction. Elucidation of the pressure induced structural changes and its influence on the PMV requires further investigation.

Acknowledgment. This work was supported by Grants-in-Aid for Scientific Research and for Young Scientists (B) (22750015) from the Ministry of Education, Culture, Sport, Science, and Technology in Japan, and for the Core Research for Evolutional Science and Technology (CREST) “High Performance Computing for Multiscale and Multiphysics Phenomena” from the Japan Science and Technology Agency.

References and Notes

- (1) Gekko, K.; Noguchi, H. *J. Phys. Chem.* **1979**, *83*, 2706–2714.
- (2) Gekko, K.; Hasegawa, Y. *Biochemistry* **1986**, *25*, 6563–6571.
- (3) Chalikian, T. V.; Totrov, M.; Abagyan, R.; Breslauer, K. *J. Mol. Biol.* **1996**, *260*, 588–603.
- (4) Tamura, Y.; Gekko, K. *Biochemistry* **1995**, *34*, 1878–1884.
- (5) Kamiyama, T.; Gekko, K. *Chem. Lett.* **1997**, 1063–1064.
- (6) Filfil, R.; Chalikian, T. V. *J. Mol. Biol.* **2000**, *299*, 827–842.
- (7) Seemann, H.; Winter, R.; Royer, C. A. *J. Mol. Biol.* **2001**, *307*, 1091–1102.
- (8) Imai, T.; Kovalenko, A.; Hirata, F. *J. Phys. Chem. B* **2005**, *109*, 6658–6665.
- (9) Yu, I.; Takayanagi, M.; Nagaoka, M. *J. Phys. Chem. B* **2009**, *113*, 3543–3547.
- (10) Kirkwood, J. G.; Buff, F. P. *J. Chem. Phys.* **1951**, *19*, 774–777.
- (11) Ben-Naim, A. *Statistical Thermodynamics for Chemist and Biochemist*; Plenum Press: New York, 1992.
- (12) Kitahara, R.; Yamada, H.; Akasaka, K.; Wright, P. E. *J. Mol. Biol.* **2002**, *320*, 311–319.
- (13) Yu, I.; Jindo, Y.; Nagaoka, M. *J. Phys. Chem. B* **2007**, *111*, 10231–10238.
- (14) Nagaoka, M.; Yu, I.; Takayanagi, M. In *Proteins: Energy, Heat and Signal Flow*; Leitner, D. M. Straub, J. E., Eds.; CRC: Boca Raton, FL, 2009.
- (15) Case, D. A.; Darden, T. A.; Cheatham, T. E.; Simmerling, C. L.; Wang, J.; Duke, R. E.; Luo, R.; Crowley, M.; Walker, R. C.; Zhang, W.; Merz, K. M.; Wang, B.; Hayik, S.; Roitberg, A.; Seabra, G.; Kolossvary, I.; Wong, K. F.; Paesani, F.; Vanicek, J.; Wu, X.; Brozell, S. R.; Steinbrecher, T.; Gohlke, H.; Yang, L.; Tan, C.; Mongan, J.; Hornak, V.; Cui, G.; Mathews, D. H.; Seetin, M. G.; Sagui, C.; Babin, V.; Kollman, P. A. *AMBER10*; University of California: San Francisco, CA, 2008.
- (16) Duan, Y.; Wu, C.; Chowdhury, S.; Lee, M. C.; Xiong, G.; Zhang, W.; Yang, R.; Cieplak, P.; Luo, R.; Lee, T.; Caldwell, J.; Wang, J.; Kollman, P. A. *J. Comput. Chem.* **2003**, *24*, 1999–2012.
- (17) Jorgensen, W. L.; Chandrasekhar, J.; Madura, J. D.; Impey, R. W.; Klein, M. L. *J. Chem. Phys.* **1983**, *79*, 926–935.
- (18) Berendsen, H. J. C.; Postma, J. P. M.; van Gunsteren, W. F.; Dinola, A.; Haak, J. R. *J. Chem. Phys.* **1984**, *81*, 3684–3690.
- (19) Darden, T.; York, D.; Pedersen, L. *J. Chem. Phys.* **1993**, *98*, 10089–10092.
- (20) Ryckaert, J. P.; Cicotti, G.; Berendsen, H. J. C. *J. Computat. Phys.* **1977**, *23*, 327–341.
- (21) Chai, C.; Jhon, M. *Mol. Sim.* **2000**, *23*, 257–574.
- (22) Refaei, M.; Tezuka, T.; Akasaka, K.; Williamson, M. P. *J. Mol. Biol.* **2003**, *327*, 857–865.
- (23) Dadarlat, V. M.; Post, C. B. *J. Phys. Chem. B* **2001**, *105*, 715–724.
- (24) Dadarlat, V. M.; Post, C. B. *Biophys. J.* **2006**, *91*, 4544–4554.
- (25) Gekko, K. *Netsu Sokutei* **2004**, *31*, 186–193.
- (26) Jorgensen, W. L.; Jenson, C. J. *Comput. Chem.* **1998**, *19*, 1179–1186.

JP1043267